Available online at www.sciencedirect.com
ScienceDirect
C. R. Physique 9 (2008) 161–168
COMPTES RENDUS PHYSIQUE
http://france.elsevier.com/direct/COMREN/

Recent developments in terahertz optoelectronics/Développements récents en optoélectronique térahertz

THz near-field measurements of metal structures

Aurèle J.L. Adam [a], Janne M. Brok [a], Paul C.M. Planken [a,*], Min Ah Seo [b], Dai Sik Kim [b]

[a] *Delft University of Technology Delft, Department of Imaging Science and Technology, Faculty of Applied Sciences, Lorentzweg 1, 2628 CJ Delft, The Netherlands*

[b] *School of Physics, Seoul National University, Seoul 151-747, Republic of Korea*

Available online 9 January 2008

Abstract

We report on electro-optic measurements of THz electric fields in the near-field of metal structures lying on GaP electro-optic sampling crystals. With (110) oriented crystals, the x or y component of the THz electric field is measured, whereas with a (001) oriented crystal, the z-component is measured. With an estimated spatial resolution of 20 μm, the technique allows us to map the field on a scale, orders of magnitude smaller than the spatial dimensions of these structures. We illustrate the technique by showing results of measurements of the THz electric field in a plane underneath a metal sphere and a single square hole in a metal foil. The technique provides us with a wealth of information on the time-evolution of light fields near metal structures. ***To cite this article: A.J.L. Adam et al., C. R. Physique 9 (2008).***

Résumé

Cartographie en champ proche du champ THz diffracté par des structures métalliques. Nous décrivons des mesures électro-optiques de champs électriques dans le domaine THz dans la région de champ proche de structures métalliques déposées sur des substrats de phosphure de gallium (GaP) électro-optiques. En utilisant des cristaux orientés (110), les composantes x ou y du champ électrique THz sont mesurées tandis que l'orientation cristallographique (001) permet de déterminer la composante z du champ. Ainsi, nous pouvons cartographier le champ avec une résolution spatiale de l'ordre de 20 μm, plus petite de plusieurs ordres de grandeur que les dimensions des structures métalliques. Pour illustrer cette technique et ses performances, nous présentons des résultats concernant le champ mesuré dans un plan situé sous une sphère métallique et sous une feuille métallique comprenant une ouverture carrée. Grâce à une technique d'échantillonnage, ce type de mesures apporte de nombreuses informations sur l'évolution temporelle du champ proche diffracté. ***Pour citer cet article : A.J.L. Adam et al., C. R. Physique 9 (2008).***

Keywords: Terahertz; Near field; Terahertz electric field

Mots-clés : Térahertz ; Champ proche ; Champ électrique THz

1. Introduction

In recent years, THz imaging has appeared as a new tool to study the interior of many objects that are normally opaque to visible light [1–8]. An important advantage of THz radiation is that it is non-ionizing at low power levels

* Corresponding author.
E-mail addresses: a.j.l.adam@tudelft.nl (A.J.L. Adam), J.M.Brok@tudelft.nl (J.M. Brok), p.c.m.planken@tudelft.nl (P.C.M. Planken), minahseo@phya.snu.ac.kr (M.A. Seo), dsk@phya.snu.ac.kr (D.S. Kim).

1631-0705/$ – see front matter
doi:10.1016/j.crhy.2007.07.005

due to the low photon energy, and can thus perhaps replace imaging equipment that uses potentially harmful radiation, in a selected number of imaging applications. Many of these imaging techniques are based on terahertz time-domain spectroscopy (THz-TDS), a technique capable of measuring the electric field of an ultrashort, broadband THz pulse. Recently, a number of imaging techniques, aimed at increasing the spatial resolution of THz imaging to dimensions smaller than the wavelength, was reported. All these THz microscope techniques have in common that they are based on either a sub-wavelength source or a sub-wavelength detector. They include the use of apertures, [9–12], metal tips, [13–17], or the use of a focused laser to locally generate THz radiation in a sub-wavelength area [18]. THz sub-wavelength microscopes are potentially highly interesting for biological applications, although this probably requires expanding the useful frequency range of these devices to higher THz frequencies where resonances of biological molecules in solution are plentiful. At lower THz frequencies (<5 THz), these microscopes can, however, be used to measure lattices resonances of small molecular crystals, which do show characteristic spectroscopic fingerprints in this frequency region [19–21]. With one exception, [15], THz sub-wavelength micro-spectroscopy has not been demonstrated yet, perhaps because at low terahertz frequencies even lattice resonances of molecular crystals are weak compared to their counterparts at high THz frequencies.

The ability to study THz electric fields at sub-wavelength dimensions is not only useful for biological applications. In general, there is a great interest in studying electromagnetic phenomena near all kinds of structures such as holes, slits and other objects. The study of these structures, mostly at visible to near-infrared wavelengths, has led to many exciting observations, such as the extraordinary transmission of light by hole arrays in metal films [22,23]. One problem associated with these measurements is that it is difficult to measure these phenomena at scales smaller then the wavelengths involved, let alone with a sub-oscillation period temporal resolution, although a successful measurement was recently reported [24]. Since Maxwell's equations are scale invariant, and assuming that the material properties are not too much frequency dependent, THz radiation would be ideally suited to study these phenomena. This is because, as we will show below, it's relatively easy to obtain a sub-wavelength spatial resolution at THz frequencies. Using THz-TDS, an additional advantage is that these experiments allow us to obtain both phase and amplitude information in an ultra-wide bandwidth. A practical advantage is that the fabrication of sub-wavelength devices is much less demanding at THz frequencies than in the visible frequency range. A number of *far-field* experiments on the transmission of single holes or hole arrays has already been carried out in the recent past [25–28]. However, a detailed study of the *near-field* of these structures, essential for understanding the physics which lies at the heart of, for example, the extraordinary transmission of light by metal hole arrays, is mostly lacking.

In this article, we present measurements of the THz near-field on metal structures, using near-field electro-optic detection in GaP crystals, with a focused probe beam. In our measurements, a focused THz beam is incident on a sample such as a metal sphere or a hole in a metal foil, lying on the GaP crystal. By using the appropriate crystal orientation, we can measure the time-evolution of the x, y, and z components of the THz electric field in a plane underneath the object, with a spatial resolution of 20 μm. For the hole, we show the presence of strong evanescent fields localized near the edges of a hole, for wide frequency range. For the sphere, we observe the development of a z-component in the 'shadow' region of the sphere, associated with the THz wavefront diffracting around it. In both experiments, due to the broadband nature of the THz pulses, we obtain information on the field both for wavelengths much longer, and for wavelengths on the order of or shorter than the typical dimensions of the hole and the sphere.

2. Experimental considerations

2.1. The setup

The setup used to measure the near electric field of metal structures is shown in Fig. 1. THz pulses are generated in a GaAs photoconductive switch modulated with a 50 kHz square wave voltage [29]. After being filtered by a wire-grid polarizer, they are used to illuminate a metal sample lying on a GaP electro-optic (EO) detection crystal, which in turn is mounted on a xy computer-controlled, piezo-electric translation stage. From below, a counter propagating synchronized probe laser pulse is focused to the front surface of the EO crystal using a reflective objective. The probe beam is optically delayed by sending the beam through an in-plane retro-reflector mounted on a loudspeaker which oscillates at 50 Hz. Due to the electro-optic effect, the THz electric field elliptically polarizes the probe beam which is reflected from the front surface of the crystal, and sent to a standard differential detection setup. It can be shown that the signal from the differential detector setup is linearly proportional to the THz electric field, for small values of the

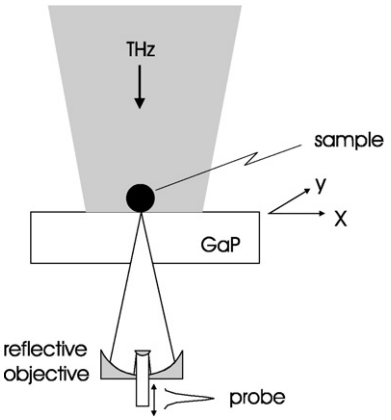

Fig. 1. Schematic of the setup used to measure the THz near-field of small metal objects. A metal sphere (black) is drawn as an example. The crystal with the object can be raster scanned with respect to the probe/THz beam.

electric field. Two different EO crystals are used. To measure the z-component of the electric field, a (001) oriented GaP crystal is used. This crystal is coated with a Ge/SiO_2 layer to maximize the reflection of the probe beam, and to prevent any probe light from reaching the samples lying on top of the crystal. To measure the x and y components, a (110) oriented crystal is used. This crystal is also coated, but with a multi-layer dielectric coating to maximize the probe reflection and to prevent probe light from reaching the samples. The coatings on the two crystals are different only to allow a comparison between the two. Both were found to be suitable. The signal from the differential detector is sent through a lock-in amplifier using a reference frequency of 50 kHz, which corresponds to the modulation frequency with which the bias voltage on the GaAs emitter is modulated. The signal from the lock-in is fed through a 10 kHz low-pass filter and then sent to a digital signal processor for further analysis. The crystal with the sample is raster scanned and for each pixel, a full, 25 ps long THz electric-field transient is measured.

2.2. Optimizing the EO crystal orientation

In general, the EO detection efficiency is a function of the crystal orientation with respect to the THz and probe beam polarizations [30–32]. For a (110) crystal orientation, and assuming that the probe beam and the THz beam both propagate along the (110) crystal axis, it can be shown that the differential signal is given by [33]:

$$\Delta I(\alpha, \varphi) = I_{\mathrm{p}} \frac{\omega n^3 E_{\mathrm{THz}} r_{41} L}{2c} [\cos\alpha \sin 2\varphi + 2 \sin\alpha \cos 2\varphi] \tag{1}$$

E_{THz} is the THz electric field, L the crystal length, I_{p} the probe intensity, c the velocity of light in vacuum, ω the angular frequency of the probe pulse, n the refractive-index of the crystal and r_{41} the electro-optic coefficient. The angles α and φ are defined in Fig. 2(a). Although perhaps not immediately obvious from Eq. (1), it is easy to show that when the crystal is optimized to detect a component of the electric field, rotation of the crystal by 90 degrees renders it sensitive to the field component perpendicular to it. This is how in the experiment we detect the x and the y component of the electric field. First, assuming that the probe and incident THz polarizations are parallel, when there is no sample on the EO crystal, the crystal is rotated until a maximum in the signal is observed. This signal represents the 'x' component and is identical to the polarization of the incident THz beam. The sample is then placed on the EO crystal and xy-rasterscans of the assembly are performed. To measure the y component of the field, the crystal is simply rotated by 90 degrees, while the sample is prevented from being rotated along with it.

For a (001) crystal, it can be show that the differential signal is given by:

$$\Delta I(\varphi) = I_{\mathrm{p}} \frac{\omega n^3 E_{\mathrm{THz}} r_{41} L}{c} \cos(2\varphi) \tag{2}$$

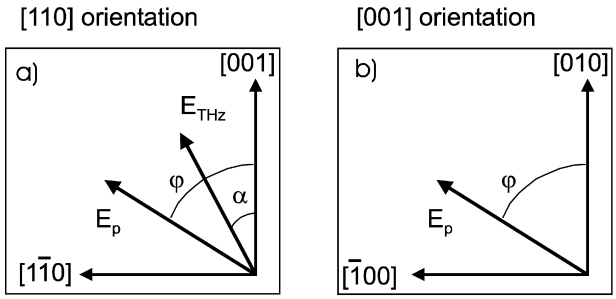

Fig. 2. Schematic of the EO crystal orientations and THz and probe laser polarizations relevant to the measurements of the near-electric field. In (a), the [110] axis points towards the reader. In (b) the [001] axis points towards the reader. In (b) the THz electric field is assumed to be parallel to the [001] axis.

where the angle φ is defined in Fig. 2(b). Here, optimization of the signal is obtained by rotating the crystal until a maximum is observed. Interestingly, for both crystal orientations, the maximum differential signal that be obtained is given by

$$\Delta I_{\max}(\varphi) = I_{\mathrm{p}} \frac{\omega n^3 E_{\mathrm{THz}} r_{41} L}{c} \tag{3}$$

In principle therefore, the signals from both crystals can directly be compared, without the need for a scaling factor that would take any difference in sensitivity into account. In practice, the different coatings on the front surface of the two crystals, have different reflectivities, giving rise to differences in the absolute reflected probe beam power on the detector, and thus to differences in the absolute signals for identical THz electric-field strengths. Experimentally, when we wish to measure the z-component of the field, we have to replace the (110) crystal with the (001) crystal.

We note that alternatively, it is also possible to use a (111) oriented EO-crystal for the detection of the x and y components of the field [8]. In this case, by choosing a proper polarization for the probe beam, information on both the E_x and the E_y components is *simultaneously* encoded on the probe beam. A half-wave plate, placed after the crystal, is rotated to select either the E_x, or the E_y component. No rotation of the *detection crystal* would be required, considerably simplifying the setup. However, the disadvantage of the use of the (111) crystal is that compared to the (001) and the (110) crystal orientations, the maximum EO signal is 18% lower. Since the near-field signals are generally small, we have decided to use the (110) crystal orientation for the detection of E_x and E_y.

3. Results and discussion

3.1. The sphere

In Fig. 3 we plot the peak-amplitude of the z-component of the THz electric field, measured in a plane directly underneath a 500 μm diameter brass sphere, lying on a 65 μm thick (001) oriented GaP crystal. The picture represents an 51×51 pixel measurement with a total scan area of 0.5×0.5 mm^2. In the figure, the projection of the circumference of the sphere on the plane underneath the sphere is indicated by the white circle. A dipole-like pattern consisting of two lobes is visible with a region of zero field in between. The polarization direction of the incident THz pulse is in the direction of the dipole-like pattern. Although not visible in the contour plot, the fields in the two lobes have opposite polarity. This is can clearly be seen in left part of the figure where we show the THz electric field as a function of time, measured at the two locations indicated by the arrows. Clearly, the two curves are more or less mirror images of each other as is expected of the z-component of the field of a dipole-like structure. The peak amplitude, however, conveys little information on the *time-evolution* of the field in the neighborhood of the sphere. For this, we plot in Fig. 4 the z-component of the THz electric field of the pulse, for three different times in the evolution of the field.

The white and black regions in this figure now represent positive and negative z-components of the THz electric field respectively. The second thing to notice in Fig. 4 (and also in Fig. 3), is that the measured z-component of the field is strongest in the region behind the sphere, in it's 'shadow'. This is clearly the result of diffraction of the light by the sphere which causes the light to bend around it. As time progresses, the regions of high field can be seen to move towards the center of the circle and to decrease in area. In the last frame, at $t = 4.2$ ps, a positive (negative)

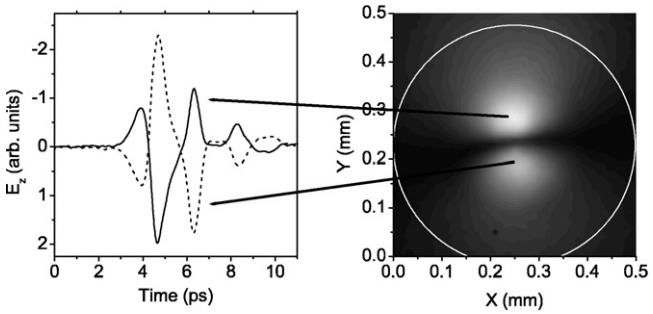

Fig. 3. Right: Spatial distribution of the maximum THz electric-field peak-amplitude $|E_z|_{\max}$, measured in a plane underneath a 500 μm diameter sphere. Left: THz electric fields $E_z(t)$ as a function of time measured at the two locations indicated by the arrows. The projection of the circumference of the sphere on the electro-optic crystal is indicated by the white circle.

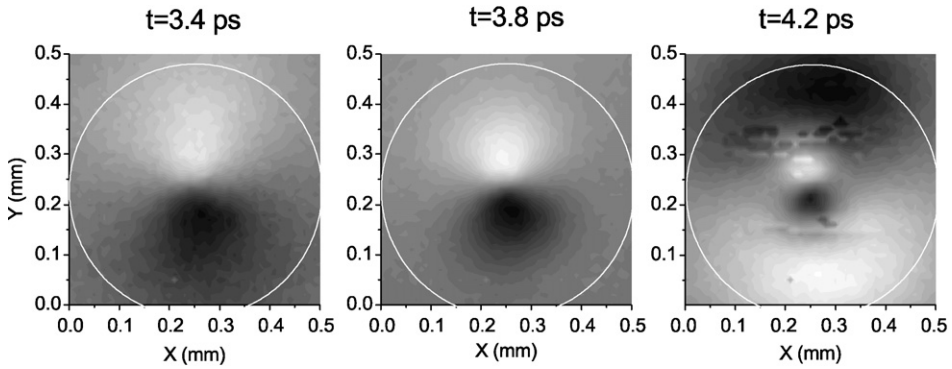

Fig. 4. Spatial distribution of the electric field $E_z(t)$ of a THz pulse, measured at three different times in a plane underneath a 0.5 mm diameter brass sphere. White and black represent positive and negative z-components of the pulse respectively. For the grey-scale encoding, each of the three frames is separately normalized. The irregularities observed in the right most graph are caused by the reduced THz amplitude of the signal in this time frame which causes (unwanted) background noise to become more visible.

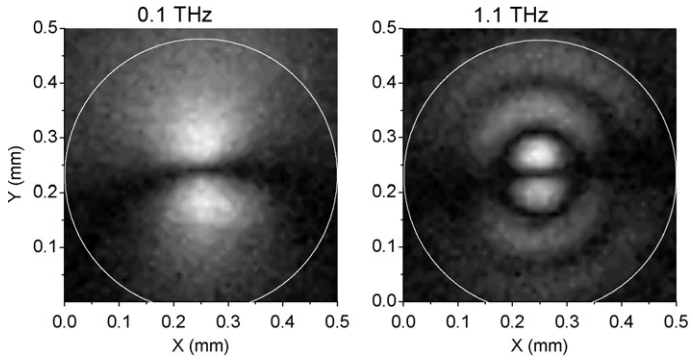

Fig. 5. Spatial distribution of the THz spectral amplitude $|E_z(\omega)|$ at two different frequencies of $\omega/(2\pi) = 0.1$ THz (left) and $\omega/(2\pi) = 1.1$ THz (right), calculated from the measured z-component of the THz electric field in a plane underneath the sphere.

z-component emerges from the edge of the sphere, following the negative (positive) field of the first part of the THz pulse visible at $t = 3.4$ ps and at $t = 3.8$ ps. Note that it is probable that the field, located on portions of the sphere which are furthest from the EO crystal, is not measured as efficiently as the field on the sphere near the contact point between the sphere and the crystal. This means that the field distribution visible in the figure may not be an exact representation of the THz field on the sphere. Nevertheless, the measurement does give an excellent impression of generation and evolution of the near-field of the sphere which is illuminated with a THz pulse. The THz pulses measured in our THz-TDS setup, contain wavelengths both larger and shorter than the sphere diameter. In Fig. 5,

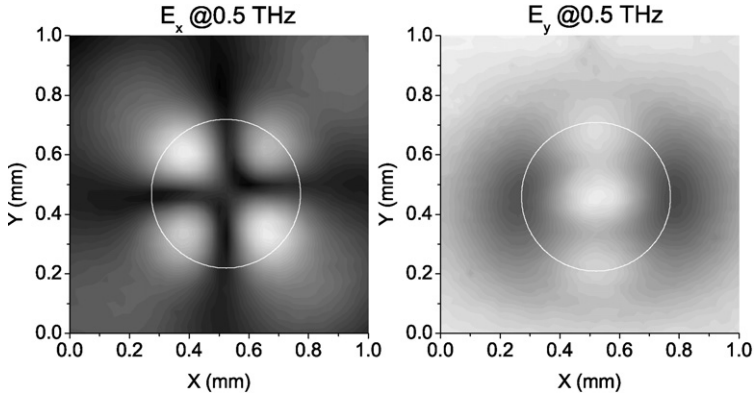

Fig. 6. Spatial distribution of the spectral amplitude $|E_x(\omega)|$ (left) and $|E_y(\omega)|$ (right) at $\omega/(2\pi) = 0.5$ THz of the THz electric field measured in a plane underneath the metal sphere. The E_y measurement does not show much contrast since the incident electric field is also clearly present as a strong background around the sphere. In both pictures, black indicates zero amplitude, white indicates maximum amplitude.

we plot the amplitude of the field measured underneath the sphere, at frequencies of 0.1 THz and 1.1 THz. At 0.1 THz, the intensity distribution resembles that of a static dipole, which has two lobes in the polarization direction of the incident THz pulse. Note that 0.1 THz corresponds to a wavelength of 3 mm, which is 6 times larger than the sphere diameter. At 1.1 THz, corresponding to a wavelength of 273 μm, the picture looks dramatically different. Now, instead of a dipole-like pattern, semi-circular white and dark bands are observed, indicating the presence of THz standing waves. Although not shown here, the location of the bands is a function of frequency, with the bands moving towards the center of the circle for increasing frequency.

The ability of our setup to measure the E_x and E_y components in addition to the E_z components, is illustrated in Fig. 6 where we plot the amplitude of these two components at a frequency of 0.5 THz. The measurement corresponds to a 41×41 pixel image having a total scan range of 1×1 mm^2. As before, the white circle represents the projection of the circumference of the sphere on the plane underneath the sphere. The measurement of the E_x component shows four lobes, whereas the measurement of the E_y shows enhanced light regions under the sphere and some regions where the amplitude is lower. Note that the incident THz polarization is in the y direction, which explains why this measurement is not 'background-free': The white regions surrounding the sphere represent the incident y-polarized THz electric field. It is interesting to note that underneath the sphere, the amplitude appears to be enhanced with respect to the amplitude some distance away from the sphere. Such a field enhancement is in fact expected for curved metal objects in an electric field.

3.2. The square hole

In Fig. 7, we plot the amplitude of the z-component of the electric field, measured in a plane underneath a 80 μm thick metal foil with a 200×200 μm^2 sized square hole, at 0.15, 0.5, 1.0, and 1.5 THz. The foil is placed onto the detection crystal and since the foil is not perfectly flat we estimate that there exists a gap of about 50–100 μm between the foil and the crystal at the location of the hole. At 0.15 THz, corresponding to a wavelength of 2000 μm, which is 10 times larger than the hole diameter, a clear dipole-like pattern is visible with its main axis in the y direction. Evidently, even for wavelengths this long, the field is able to generate an evanescent E_z component on the shadow-side of the metal. The spatial extent of the measured z-component is a strong function of frequency as can be seen from Fig. 7. When the frequency increases, the dipole-like pattern shrinks in area and becomes more localized near the edges of the hole. Note that the highest frequency of 1.5 THz for which we show results is ten times higher than the lowest frequency of 0.15 THz for which we show results, a result made possible by the intrinsically broadband nature of THz-TDS. Strictly speaking, our experimental setup does not measure the electric field in a single plane behind the object. More accurately, the measured signal is a spatial integral in the z-direction over a certain interaction length inside the electro-optic crystal, starting from the surface where the object is located. (To be more precise, we sample the field in a *volume* inside the crystal as the probe beam also has a finite diameter. We currently ignore the finite diameter of the probe beam, since measurements on the near-field of a metal tip apex using a similar setup, show

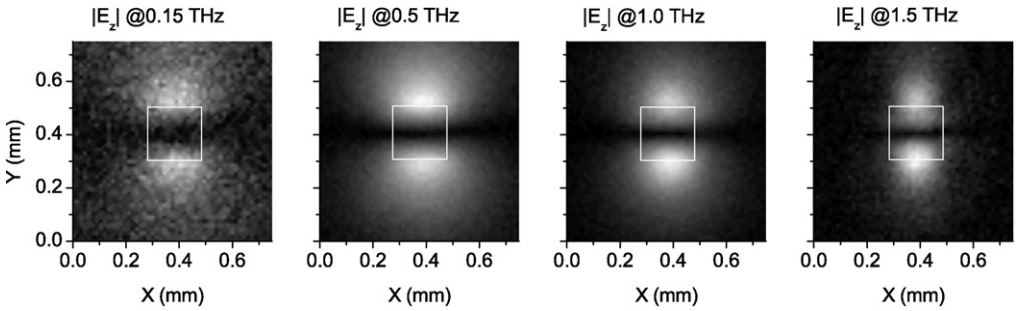

Fig. 7. Spatial distribution of the spectral amplitude $|E_z(\omega)|$ of the THz electric field, measured in a plane underneath a 200×200 μm^2 square hole in an 80 μm thick metal foil, at four different frequencies, indicated in the figure. The white square outlines the hole in the foil.

that the beam diameter is smaller than 7 μm over a considerable distance inside the crystal [13].) We therefore do not a priori know whether the results shown in Fig. 7 reflect the limited spatial resolution of our setup, or the real shape of the evanescent field. Fortunately, additional measurements on metal foils deposited directly onto the detection crystal (not shown here), show electric fields much more strongly localized near the edges of the square holes, compared to the results in Fig. 7. This means that the shape of the dipole-like pattern is not a consequence of a limited spatial resolution but of the shape of, and distance to the hole. It also implies that the in-plane spatial distribution of the near-field of the hole is a strong function of the distance to the foil.

Our estimate of a spatial resolution in our measurement of the z-component of the field of about 20 μm is based on the sharpness of the structures observed in the 2D images of the electric field. It is also confirmed by measurements on the near-field of holes in metal films (not shown here) where we can separate fields emerging from closely spaced neighboring holes. It is probable that the spatial resolution for E_x and E_y is different. This can be understood from the fact, that the z-component of the field is mostly evanescent, and can thus not propagate into the z direction, which is the propagation direction of the probe beam. The spatial decay of the z-component into the crystal is, in most cases shorter than the crystal thickness. The focussed probe beam thus mostly samples the z-component in a region close to the object. The y-component on the other hand, is mostly a propagating component which can easily propagate along with the probe pulse. At the entrance of the crystal however, the probe diameter is larger than at the backplane where the sphere is located. At the entrance, the probe beam thus samples a larger area of the THz field, reducing the spatial resolution. The spatial resolution of the x and y components is certainly better than 50 μm and attempts to more accurately determine the spatial resolution are currently under way.

In conclusion, we have presented a method, based on THz-TDS, to measure the THz near-field of metal objects placed on the surface of GaP electro-optic crystals. We find that a focussed probe beam is capable of 'reading' the near-field of these structures with a sub-wavelength spatial resolution of several tens of microns. Using (001) and (110) oriented GaP crystals, both the z, and the x and y components of the field can be obtained. Examples of measurements on a sphere show the ability of the method to observe standing waves. Measurement of the near-field of a square hole in a metal foil show a frequency-dependent, dipole-like pattern on the shadow side of the foil. Signals are observed for wavelengths ten times larger than the hole width. Our method can be applied to the study of the near-fields of many structures, such as single holes and hole arrays in metal foils.

Acknowledgements

This work was performed as part of the research program of the "Stichting voor Fundamenteel Onderzoek der Materie (FOM)", which is financially supported by the "Nederlandse Organisatie voor Wetenschappelijk Onderzoek (NWO) and as part of the EU TERANOVA Program (RCN-71835)". Research support from the Korean government (Korean Science and Engineering Foundation, Ministry of Science and Technology, Ministry of Commerce and Industry, and the Research Council of the City of Seoul) is also acknowledged.

References

[1] B.B. Hu, M.C. Nuss, Opt. Lett. 20 (1995) 1716–1718.

[2] D.M. Mittleman, M. Gupta, R. Neelamani, R.G. Baraniuk, J.V. Rudd, M. Koch, Appl. Phys. B 68 (1999) 1085–1094.
[3] Q. Wu, T.D. Hewitt, X.-C. Zhang, Appl. Phys. Lett. 69 (1996) 1026–1028.
[4] F. Rutz, T. Hasek, M. Koch, H. Richter, U. Ewert, Appl. Phys. Lett. 89 (2006) 221911/1–3.
[5] D.M. Mittleman, S. Hunsche, L. Boivin, M.C. Nuss, Opt. Lett. 22 (1997) 904–906.
[6] B. Ferguson, X.-C. Zhang, Nature Mater. 1 (2002) 26–33.
[7] D. Mittleman, Sensing with Terahertz Radiation, Springer, Heidelberg, 2003.
[8] N.C.J. van der Valk, W.A.M. van der Marel, P.C.M. Planken, Opt. Lett. 30 (2005) 2802–2804.
[9] S. Hunsche, M. Koch, I. Brener, M.C. Nuss, Optics Commun. 150 (1998) 22–26.
[10] K. Ishihara, T. Ikari, H. Minamide, J. Shikata, K. Ohashi, H. Yokoyama, H. Ito, Jpn. J. Appl. Phys. 44 (2005) L929–L931.
[11] Q. Chen, X.-C. Zhang, IEEE J. Sel. Top. Quantum Electr. 7 (2001) 608–614.
[12] O. Mitrofanov, M. Lee, J.W.P. Hsu, I. Brener, R. Harel, J.F. Federici, J.D. Wynn, L.N. Pfeiffer, K.W. West, IEEE J. Sel. Top. Quantum Electr. 7 (2001) 600–607.
[13] N.C.J. van der Valk, P.C.M. Planken, Appl. Phys. Lett. 81 (2002) 1558–1560.
[14] P.C.M. Planken, N.C.J. van der Valk, Opt. Lett. 29 (2004) 2306–2308.
[15] P.C.M. Planken, C.E.W.M. van Rijmenam, R.N. Schouten, Semicond. Sci. Technol. 20 (2005) S121–S127.
[16] H.-T. Chen, R. Kersting, G.C. Cho, Appl. Phys. Lett. 83 (2003) 3009–3011.
[17] F. Buersgens, R. Kersting, H.-T. Chen, Appl. Phys. Lett. 88 (2006) 112115/1–3.
[18] R. Lecaque, S. Grésillon, N. Barbey, R. Peretti, J.-C. Rivoal, C. Boccara, Opt. Commun. 262 (2006) 125–128.
[19] M.B. Johnston, L.M. Herz, A.L.T. Khan, A. Köhler, A.G. Davies, E.H. Linfield, Chem. Phys. Lett. 377 (2003) 256–262.
[20] M. Walther, B.M. Fischer, P. Uhd Jepsen, Chem. Phys. 288 (2003) 261–268.
[21] Y.C. Shen, P.C. Upadhya, E.H. Linfield, A.G. Davies, Appl. Phys. Lett. 82 (2003) 2350–2352.
[22] T.W. Ebbesen, H.J. Lezec, H.F. Ghaemi, T. Thio, P.A. Wolff, Nature 391 (1998) 667–669.
[23] W.L. Barnes, A. Dereux, T.W. Ebbesen, Nature 424 (2003) 824–830.
[24] K.G. Lee, et al., Nature Photonics 1 (2007) 53–56.
[25] J. Gómez Rivas, M. Kuttge, P. Haring Bolivar, H. Kurz, J.A. Sánchez-Gil, Phys. Rev. Lett. 93 (2004) 256804/1–4.
[26] X. Shou, A. Agrawal, A. Nahata, Opt. Express 13 (2005) 9834–9840.
[27] A.K. Azad, Y. Zhao, W. Zhang, M. He, Opt. Lett. 31 (2006) 2637–2639.
[28] A. Agrawal, H. Cao, A. Nahata, Opt. Express 9 (2005) 3442–3535.
[29] G. Zhao, R.N. Schouten, N. van der Valk, W.Th. Wenckebach, P.C.M. Planken, Rev. Sci. Instrum. 73 (2002) 1715–1719.
[30] N.C.J. van der Valk, W.Th. Wenckebach, P.C.M. Planken, J. Opt. Soc. Am. B 21 (2004) 622–631.
[31] L. Duvillaret, S. Rialland, J.-L. Coutaz, J. Opt. Soc. Am. B 19 (2002) 2692–2703.
[32] L. Duvillaret, S. Rialland, J.-L. Coutaz, J. Opt. Soc. Am. B 19 (2002) 2704–2715.
[33] P.C.M. Planken, H.-K. Nienhuys, H.J. Bakker, W.Th. Wenckebach, J. Opt. Soc. Am. B 18 (2001) 313–317.